Cancer Immunology, Immunotherapy (2021) 70:2035–2048
https://doi.org/10.1007/s00262-020-02840-0

ORIGINAL ARTICLE

Comparative analysis of the tumor immune-microenvironment of primary and brain metastases of non-small-cell lung cancer reveals organ-specific and *EGFR* mutation-dependent unique immune landscape

Seung Geun Song[1] · Sehui Kim[1,2] · Jaemoon Koh[1,2] · Jeemin Yim[1] · Bogyeong Han[1] · Young A. Kim[3] · Yoon Kyung Jeon[1,4] · Doo Hyun Chung[1,2]

Received: 31 August 2020 / Accepted: 21 December 2020 / Published online: 9 January 2021

Abstract

Background To evaluate the characteristics of the tumor immune-microenvironment in brain metastases of non-small-cell lung cancer (NSCLC), we investigated the immunophenotype of primary NSCLC and its brain metastasis.

Methods Expression profiling of 770 immune-related genes in 28 tissues from primary and brain metastases of NSCLC was performed using the NanoString nCounter PanCancer Immune Profiling Panel. The immune cell profiles were validated by immunohistochemistry of 42 matched samples.

Results Based on unsupervised clustering and principal component analysis of the immune-related gene expression profile, tumors were primarily clustered according to the involved organ and further grouped according to the *EGFR* mutation status. Fifty-four genes were significantly differentially expressed between primary and brain metastatic tumors. Clustering using these genes showed that tumors harboring mutated *EGFR* tended to be grouped together in the brain. Pathway analysis revealed that various immune-related functions involving immune regulation, T cell activity, and chemokines were enriched in primary tumors compared to brain metastases. Diverse immune-related pathways were upregulated in brain metastases of *EGFR*-mutated compared to *EGFR*-wild-type adenocarcinoma, but not in primary tumors. The interferon-γ-related gene signature was significantly decreased in brain metastases. The anti-inflammatory markers *TOLLIP* and *HLA-G* were upregulated in brain metastases. The proportions of most immune cell subsets were decreased in brain metastases, but those of macrophages and CD56dim-NK-cells were increased, as was the ratios of $CD163^+$M2- to $iNOS^+$M1-macrophages and $NCR1^+$NK-cells to $CD3^+$T cells.

Conclusions Our findings illustrate the immune landscape of brain metastases from NSCLC and reveal potential therapeutic strategies targeting cellular and non-cellular components of the tumor immune-microenvironment.

Keywords Tumor immune-microenvironment · Brain metastasis · Lung cancer · Immunotherapeutic response · Immune cell profiling

Introduction

Brain metastases develop in up to 30% of patients with advanced non-small-cell lung cancer (NSCLC) [1]. Although the brain is one of the most frequent metastatic sites for lung cancer, there are few treatment options [2]. Conventional platinum-based chemotherapy has low effectiveness because of its poor blood–brain barrier permeability [3]. Several tyrosine kinase inhibitors (TKIs) are effective against central nervous system (CNS) metastases, but their use is limited to patients with targetable oncogenic

Yoon Kyung Jeon and Doo Hyun Chung contributed equally to this work.

Supplementary Information The online version contains supplementary material available at https://doi.org/10.1007/s00262-020-02840-0.

✉ Yoon Kyung Jeon
ykjeon@snu.ac.kr

✉ Doo Hyun Chung
doohyun@snu.ac.kr

Extended author information available on the last page of the article

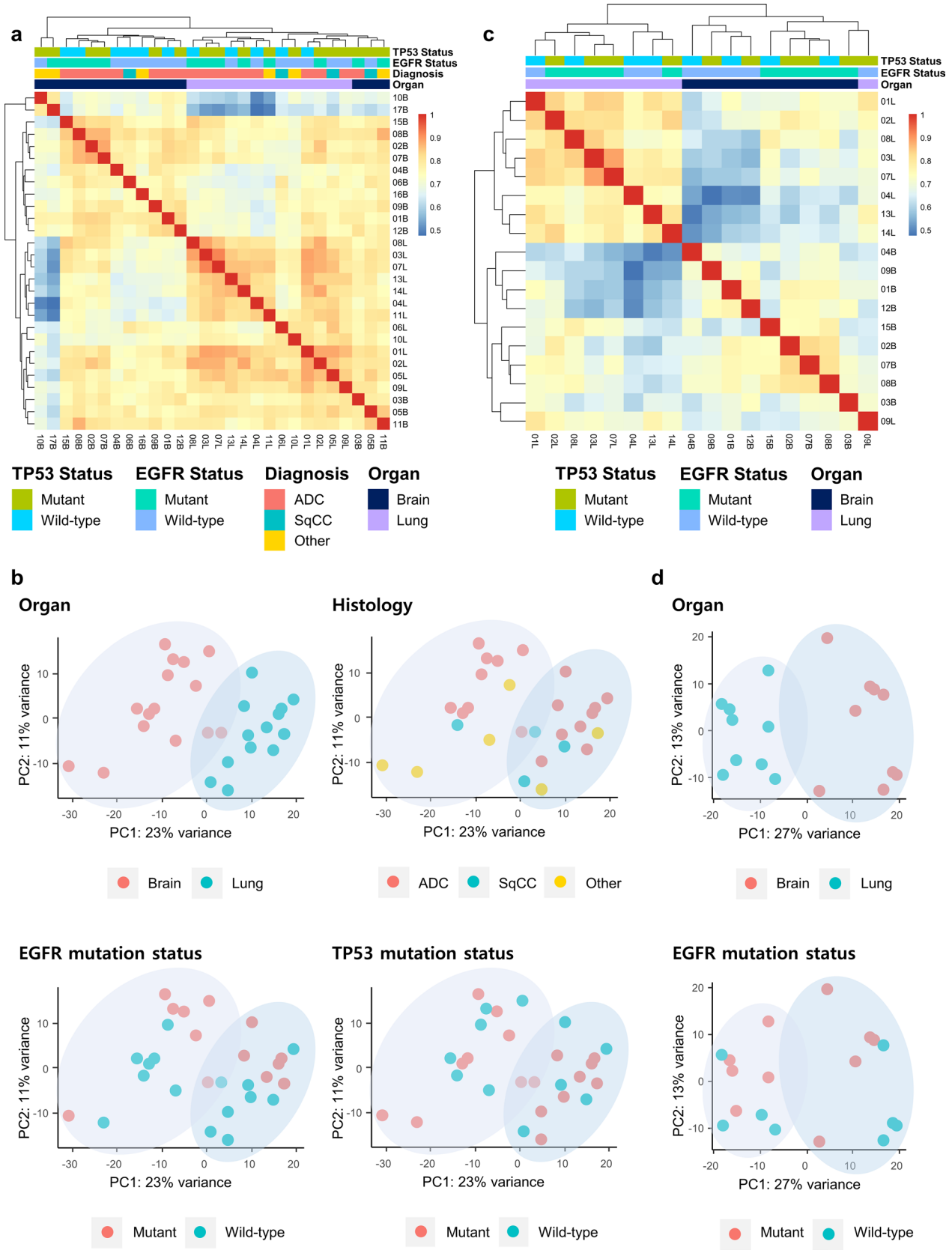
a
TP53 Status
EGFR Status
Diagnosis
Organ
TP53 Status
Mutant
Wild-type
EGFR Status
Mutant
Wild-type
Diagnosis
ADC
SqCC
Other
Organ
Brain
Lung
c
TP53 Status
EGFR Status
Organ
TP53 Status
Mutant
Wild-type
EGFR Status
Mutant
Wild-type
Organ
Brain
Lung
b
Organ
Histology
d
Organ
PC2: 11% variance
PC1: 23% variance
PC2: 13% variance
PC1: 27% variance
Brain
Lung
ADC
SqCC
Other
Brain
Lung
EGFR mutation status
TP53 mutation status
EGFR mutation status
Mutant
Wild-type
Mutant
Wild-type
Mutant
Wild-type

◂**Fig. 1** The tumor immune-microenvironment differs between the lung and brain and can be further subgrouped by *EGFR* mutation status. a-b, Correlation heatmap for unsupervised hierarchical clustering of total 28 primary NSCLC and LCBM cases (**a**) or 18 adenocarcinoma cases (**b**) based on the gene expression profile determined using the nCounter® PanCancer Immune Profiling Panel. **c** Principal component analysis (PCA) plot of the 28 samples based on the involved organ, histologic diagnosis, *EGFR* mutation status, and *TP53* mutation status. Other histologic subtypes include sarcomatoid carcinoma and salivary duct carcinoma. **d** PCA plot of the 18 adenocarcinoma cases based on organ and the *EGFR* mutation status. *ADC* adenocarcinoma; *SqCC* squamous cell carcinoma

mutations [4]. Immune-checkpoint inhibitors (ICIs) targeting the PD-1 axis show clinical efficacy in lung cancer brain metastasis (LCBM) and are important treatment options [5]. However, the response to anti-PD-1 therapy differs between primary NSCLC and LCBM [5]. These findings suggest that the tumor immune-microenvironment serves as a critical regulator of the intracranial response to ICI therapy.

The tumor immune-microenvironment encompasses various components other than tumor cells, including stromal cells, immune cells, cytokines, chemokines, and the extracellular matrix [6]. In glial tumors, pro-tumorigenic macrophages/microglia account for the majority of infiltrating immune cells and the lymphoid cells are typically suppressed by various mechanisms [7, 8]. In immunohistochemistry-based studies of LCBM with paired primary lung cancer, the amounts of tumor-infiltrating leukocytes (TILs) and PD-1-positive TILs were reduced in the brain [9, 10]. Nevertheless, the immune landscape of LCBM is still poorly understood, and an enhanced understanding of their immunobiology would improve therapeutic efficacy and lead to discovery of novel targets for immunotherapy.

To address this issue, we evaluated the tumor immune-microenvironment of patients with advanced NSCLC with brain metastases by comparative gene expression profiling of primary lung lesion and LCBM.

Materials and methods

Patient information

Twenty one patients who underwent surgery for NSCLC brain metastasis at Seoul National University Hospital (SNUH) from January 2013 to March 2018 were enrolled in the study. Clinicopathological information including age, gender, smoking history, tumor genetic status, treatments, and follow up data were retrieved from the electronic medical records. Pathologic staging was based on the 8th edition of the American Joint Committee on Cancer (AJCC) staging system.

Table 1 Clinicopathologic characteristics of patients in the NanoString study cohort and the extended cohort

Characteristic	NanoString study cohort	Extended cohort
Patient, *n*	17	21
Organ, *n*		
Lung	13	21
Brain	15	21
Age at initial diagnosis, median (range)	60 (31–77)	60 (25–77)
Sex, *n* (%)		
Female	8 (47.1)	9 (42.9)
Male	9 (52.9)	12 (57.1)
Smoking, *n* (%)		
No history of smoking	9 (52.9)	11 (52.4)
History of smoking	8 (47.1)	10 (47.6)
Histologic type, *n* (%)		
Adenocarcinoma	11 (64.7)	13 (61.9)
Squamous cell carcinoma	2 (11.8)	2 (9.5)
NSCLC, other	4 (23.5)	6 (28.6)
Stage at diagnosis, *n* (%)		
Early (IA–IIIA)	12 (70.6)	15 (71.4)
Advanced (IIIB–IV)	5 (29.4)	6 (28.6)
Molecular alteration, *n* (%)		
EGFR mutation	8 (47.1)	9 (42.9)
TP53 aberration	10 (58.8)	13 (61.9)
ALK translocation	0 (0.0)	0 (0.0)
KRAS mutation[a]	0 (0.0)	1 (4.8)
Adjuvant therapy[b], *n* (%)		
Chemotherapy	13 (76.5)	15 (71.4)
TKI therapy	1 (5.9)	1 (4.8)
Timing of brain metastasis, *n* (%)		
Synchronous	0 (0.0)	2 (9.5)
Metachronous	17 (100.0)	19 (90.5)

[a]*KRAS* mutation was screened in 12 patients

[b]Medical treatment between the initial lung surgery and subsequent brain metastatectomy

Immune-related gene expression profiling using the NanoString platform

Expression profiling of 770 immune-related genes was performed using the nCounter® PanCancer Immune Profiling Panel (NanoString Technologies Inc., Seattle, WA) [11]. Ten unstained slides of 10 µm thickness were obtained from representative formalin-fixed paraffin-embedded (FFPE) blocks of surgical specimens. Based on the corresponding hematoxylin and eosin (H&E) slide, viable tumor portion was macrodissected. After extraction, the RNA was quantified and its quality was assessed using DS 11 spectrophotometer (DeNovix Inc., Wilmington, DE) and AATI Fragment Analyzer (Agilent Technologies,

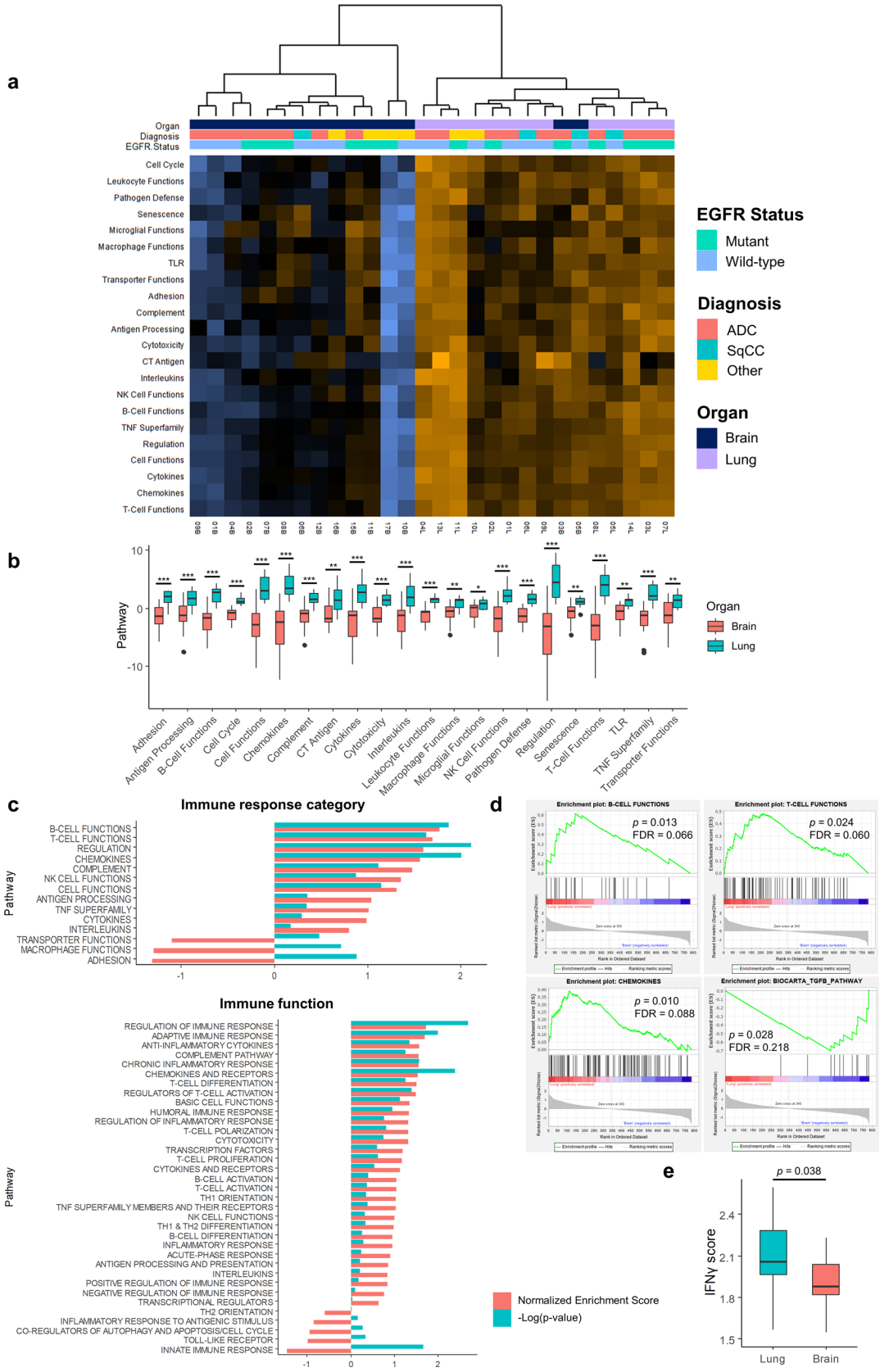
a
Organ
Diagnosis
EGFR Status
Cell Cycle
Leukocyte Functions
Pathogen Defense
Senescence
Microglial Functions
Macrophage Functions
TLR
Transporter Functions
Adhesion
Complement
Antigen Processing
Cytotoxicity
CT Antigen
Interleukins
NK Cell Functions
B-Cell Functions
TNF Superfamily
Regulation
Cell Functions
Cytokines
Chemokines
T-Cell Functions
EGFR Status
Mutant
Wild-type
Diagnosis
ADC
SqCC
Other
Organ
Brain
Lung
b
Pathway
Organ
Brain
Lung
Adhesion
Antigen Processing
B-Cell Functions
Cell Cycle
Cell Functions
Chemokines
Complement
CT Antigen
Cytokines
Cytotoxicity
Interleukins
Leukocyte Functions
Macrophage Functions
Microglial Functions
NK Cell Functions
Pathogen Defense
Regulation
Senescence
T-Cell Functions
TLR
TNF Superfamily
Transporter Functions
c
Immune response category
Pathway
B-CELL FUNCTIONS
T-CELL FUNCTIONS
REGULATION
CHEMOKINES
COMPLEMENT
NK CELL FUNCTIONS
CELL FUNCTIONS
ANTIGEN PROCESSING
TNF SUPERFAMILY
CYTOKINES
INTERLEUKINS
TRANSPORTER FUNCTIONS
MACROPHAGE FUNCTIONS
ADHESION
Immune function
Pathway
REGULATION OF IMMUNE RESPONSE
ADAPTIVE IMMUNE RESPONSE
ANTI-INFLAMMATORY CYTOKINES
COMPLEMENT PATHWAY
CHRONIC INFLAMMATORY RESPONSE
CHEMOKINES AND RECEPTORS
T-CELL DIFFERENTIATION
REGULATORS OF T-CELL ACTIVATION
BASIC CELL FUNCTIONS
HUMORAL IMMUNE RESPONSE
REGULATION OF INFLAMMATORY RESPONSE
T-CELL POLARIZATION
CYTOTOXICITY
TRANSCRIPTION FACTORS
T-CELL PROLIFERATION
CYTOKINES AND RECEPTORS
B-CELL ACTIVATION
T-CELL ACTIVATION
TH1 ORIENTATION
TNF SUPERFAMILY MEMBERS AND THEIR RECEPTORS
NK CELL FUNCTIONS
TH1 & TH2 DIFFERENTIATION
B-CELL DIFFERENTIATION
INFLAMMATORY RESPONSE
ACUTE-PHASE RESPONSE
ANTIGEN PROCESSING AND PRESENTATION
INTERLEUKINS
POSITIVE REGULATION OF IMMUNE RESPONSE
NEGATIVE REGULATION OF IMMUNE RESPONSE
TRANSCRIPTIONAL REGULATORS
TH2 ORIENTATION
INFLAMMATORY RESPONSE TO ANTIGENIC STIMULUS
CO-REGULATORS OF AUTOPHAGY AND APOPTOSIS/CELL CYCLE
TOLL-LIKE RECEPTOR
INNATE IMMUNE RESPONSE
Normalized Enrichment Score
-Log(p-value)
d
Enrichment plot: B-CELL FUNCTIONS
p = 0.013
FDR = 0.066
Enrichment plot: T-CELL FUNCTIONS
p = 0.024
FDR = 0.060
Enrichment plot: CHEMOKINES
p = 0.010
FDR = 0.088
Enrichment plot: BIOCARTA_TGFB_PATHWAY
p = 0.028
FDR = 0.218
e
p = 0.038
IFNy score
Lung
Brain

◂**Fig. 2** Brain metastasis has a suppressed and unique immunophenotype. **a** Pathway scores calculated with nSolver 4.0 and visualized as a heatmap plot. Scores are Z-transformed and displayed on the same scale. Orange, high scores; blue, low scores. **b** Pathway scores according to organ (Mann–Whitney *U* test). **c** Gene set enrichment analysis of primary lung cancer versus lung cancer brain metastasis (LCBM) using the gene sets for immune response category (upper) and immune function (lower). A positive enrichment score indicates that the gene set is enriched in primary lung cancer samples. **d** Representative enrichment plots with *P* values and false discovery rate (FDR) *q* values. **e** IFN-γ signature score (independent-sample *t* test). CT antigen, cancer/testis antigen; TLR, Toll-like receptor; *, $P<0.05$; **, $P<0.01$; ***, $P<0.001$; *ns* not significant

Santa Clara, CA). The criteria for acceptable quality were RNA concentration ≥ 20 ng/μL, total RNA ≥ 100 ng, A260/A230 ratio ≥ 1.0, and bioanalyzer peak ≥ 200 nucleotides. Raw data were processed into a signature matrix using nSolver Analysis Software version 4.0 (NanoString Technologies Inc.). The gene expression data are available at the Gene Expression Omnibus (GEO) repository under accession number GSE161116.

Clustering and differential expression analysis

Gene expression data were normalized using the DESeq2 package in R and hierarchical clustering, principal component analysis (PCA) and exploration of differentially expressed genes (DEGs) were performed [12]. Graphs were plotted using the ggplot2, pheatmap, and EnhancedVolcano packages in R.

Interferon-γ signature scoring

The interferon-γ (IFN-γ) signature score was calculated as previously described [13]. Briefly, raw gene expression counts were subjected to quantile normalization. The result was log10-transformed, and the IFN-γ signature score was calculated by averaging the values of six genes (*IDO1*, *CXCL10*, *CXCL9*, *HLA-DRA*, *STAT1*, and *IFNG*).

Pathway analysis

Gene set enrichment analysis (GSEA) was conducted using GSEA software v.4.0.3. The reference data file annotated with immunological functions for 770 genes in the nCounter® PanCancer Immune Profiling Panel was downloaded from the NanoString Technologies website (https://www.nanostring.com/products/gene-expression-panels/gene-expression-panels-overview/hallmarks-cancer-gene-expression-panel-collection/pancancer-immune-profiling-panel?jumpto=SUPPORT). These reference data, which are annotated with the immunological function and biological process categories from the Gene Ontology Consortium, were then processed to gene sets in the gene matrix file format (.gmt) for GSEA.

Based on the same predefined gene sets, immune-related pathway scores were estimated using the module in nSolver 4.0. The pathway scores were based on the first principal component of the expression data in each sample, based on the expression levels for the gene sets related to the specific pathway [14].

Immune cell deconvolution

The immune cell composition of tumor samples was characterized by the NanoString method and the Cell-type Identification by Estimating Relative Subsets of RNA Transcripts (CIBERSORT) algorithm [15, 16].

The NanoString method was carried out using nSolver 4.0. This method evaluates the abundance of 14 immune cell populations using the expression level of previously defined cell-type-specific marker genes [17].

The CIBERSORT algorithm computes relative abundance of 22 immune cell types and their statistical significance using the reference gene signature matrix (LM22) comprising 547 genes. CIBERSORT analysis was conducted on the CIBERSORT website (https://cibersort.stanford.edu/).

Immunohistochemistry

Immunohistochemistry was performed using antibodies against CD3 (Ventana Medical Systems, Tucson, AZ), NCR1 (R&D Systems, Minneapolis, MN), iNOS (Abcam, Cambridge, UK), and CD163 (Cell Marque, Rocklin, CA) with a Benchmark XT autostainer (Ventana Medical Systems). Immunohistochemistry results were evaluated by counting the number of cells with robust immunoreactivity per 10 high-power fields. As a surrogate for *TP53* mutation, immunohistochemistry for p53 (Dako, Agilent Technologies, Santa Clara, CA) was performed. Tumors were regarded to have *TP53* aberration if they exhibited p53 overexpression or null expression, as previously validated [18].

Statistical analysis

The normality of data was assessed by Kolmogorov–Smirnov test and Shapiro–Wilk test. The IFN-γ score, pathway score, and immune cell distribution between the groups were compared by independent-sample *t* test and Mann–Whitney *U* test. Immunohistochemical data were compared by Wilcoxon signed-rank test. Statistical analysis was performed using R statistical software, version 3.6.1. Two-sided *P* values <0.05 were considered statistically significant in all analyses.

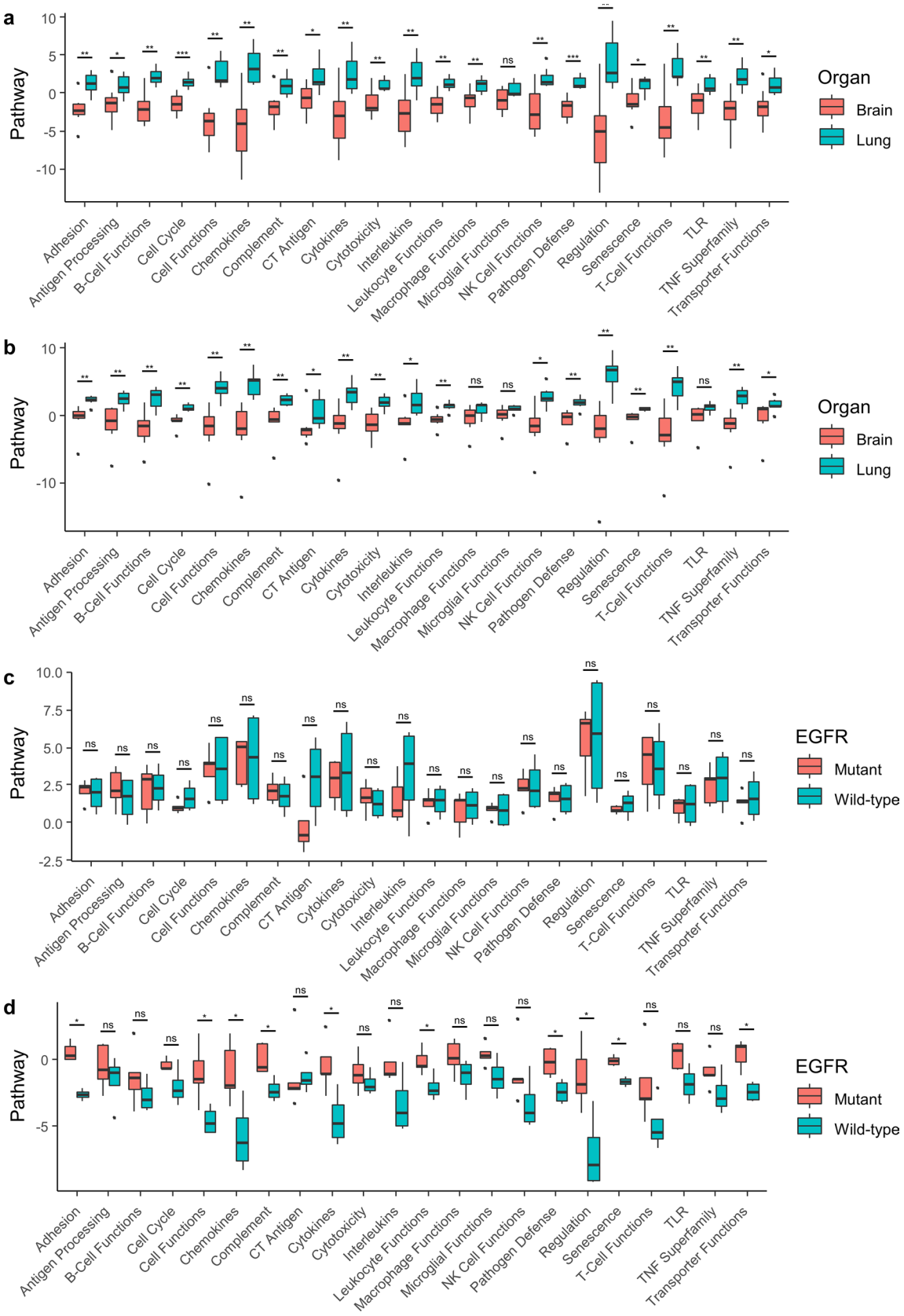
a
Pathway
Organ
Brain
Lung
b
Pathway
Organ
Brain
Lung
c
Pathway
EGFR
Mutant
Wild-type
d
Pathway
EGFR
Mutant
Wild-type
Adhesion
Antigen Processing
B-Cell Functions
Cell Cycle
Cell Functions
Chemokines
Complement
CT Antigen
Cytokines
Cytotoxicity
Interleukins
Leukocyte Functions
Macrophage Functions
Microglial Functions
NK Cell Functions
Pathogen Defense
Regulation
Senescence
T-Cell Functions
TLR
TNF Superfamily
Transporter Functions

◂**Fig. 3** Differential immune landscape according to *EGFR* mutation status. a-b, Immune-related pathway scores of primary lung tumors and LCBM cases in *EGFR* wild-type (**a**) and mutant (**b**) subgroups calculated by nSolver 4.0 (Mann–Whitney *U* test). **c** Immune scores of *EGFR* wild-type versus *EGFR* mutant primary lung adenocarcinoma samples (Mann–Whitney *U* test). **d** Immune scores of *EGFR* wild-type versus *EGFR* mutant LCBM adenocarcinoma cases (Mann–Whitney *U* test). CT antigen, cancer/testis antigen; TLR, Toll-like receptor; *, $P<0.05$; **, $P<0.01$; ***, $P<0.001$; *ns* not significant

Results

Patients' characteristics

Among the 42 tumor samples obtained from 21 patients, 28 samples satisfied the RNA quality criteria and were included in the NanoString panel analysis (Table 1). The analysis included 11 pairs of primary lung carcinoma and LCBM from the same patient, and a further unmatched two primary lung and four brain metastatic tumors. The diagnosis was adenocarcinoma in 11 patients, squamous cell carcinoma in two patients, and other NSCLCs in four patients. No patient received glucocorticoid therapy prior to surgery for brain metastases. About half of the patients harbored an *EGFR* mutation or *TP53* aberration. Among the 8 *EGFR* mutant patients in the NanoString study cohort, the detailed mutation profiles were four exon 19 deletions (E19del), three exon 21 L858R missense mutations (L858R), and one exon 20 missense mutation (S768I/V769L). None of the cases showed evidence of *ALK* translocation.

The immune cell profiling results were validated by immunohistochemistry of 42 matched primary NSCLC and LCBM samples from the extended cohort. The clinical characteristics were similar to those of the NanoString study cohort (Table 1).

Tumor immune-microenvironment of the lung and brain

Based on unsupervised hierarchical clustering of the expression levels of all immune-related genes, tumors from the lung and brain formed separate clusters (Fig. 1a). Within each organ cluster, *EGFR* wild-type and mutant cases tended to aggregate in different subgroups, but no distinct clustering pattern was observed by histology, *TP53* status, or individual patient (Fig. 1c; Supplementary Fig. 1a). Clustering of adenocarcinoma cases ($n=18$) showed that tumors were divided into groups according to the involved organ and *EGFR* mutation status (Fig. 1b and d; Supplementary Fig. 1b). These data suggest that primary lung cancer and LCBM lesions exhibit different bulk immune-related gene expression profiles, which also differs within each organ according to *EGFR* mutation status.

Immunophenotype of brain metastases

To evaluate the immune response in the lung and brain, we performed pathway analysis using nSolver 4.0. Various immune-related pathway scores were lower in LCBM compared to those of primary lung cancer; the largest differences were in the scores of immune regulation, T cell functions, and chemokine-related pathways (Fig. 2a and b).

GSEA between primary lung tumor and brain metastasis revealed that primary lung lesions were enriched for genes related to B cell functions (NES = 1.78, $P=0.013$, FDR q = 0.066), T cell functions (NES = 1.70, $P=0.024$, FDR $q=0.060$), immune regulation (NES = 1.60, $P=0.008$, FDR $q=0.092$), and chemokines (NES = 1.56, $P=0.010$, FDR $q=0.088$). In contrast, TGF-β signaling pathway was upregulated in the LCBM group (NES = 1.52, $P=0.028$, FDR $q=0.218$), suggesting an immunosuppressive microenvironment in the brain metastatic lesions (Fig. 2c and d). IFN-γ signature based on six genes has been proposed to be predictive of the clinical response to PD-1 blockade [13]. The IFN-γ signature score was lower in LCBM compared to that of primary lung tumor ($P=0.038$) (Fig. 2e). Altogether, these data show that LCBM is associated with a suppressed tumor immune-microenvironment and a reduced tumor immune response.

Immune landscape according to *EGFR* mutation status

EGFR mutation is associated with an uninflamed phenotype and weak immunogenicity [19]. Because *EGFR* mutant and wild-type cases tended to form separate clusters (Fig. 1a–d), we evaluated the effect of *EGFR* mutation on immune pathways. LCBM showed a suppressed immune response compared to the primary pulmonary lesion irrespective of *EGFR* mutation status (Fig. 3a and b). Within primary lung cancer tissues, there was no significant difference in immune pathway score according to *EGFR* mutation status (Fig. 3c, Supplementary Fig. 2a). However, diverse immune-related pathways were upregulated in LCBM cases of *EGFR*-mutated compared to *EGFR*-wild-type adenocarcinoma (Fig. 3d). A similar trend was detected for brain metastasis tissues of all histologic subtypes (Supplementary Fig. 2b). EGFR TKI affects the tumor microenvironment of lung cancer [20]. Thus, we re-analyzed the data excluding the one patient with previous TKI therapy, which showed that *EGFR* mutation was associated with increased scores of diverse immune pathways involved in chemokines ($P=0.057$), complements ($P=0.029$), cytokines ($P=0.057$), leukocyte functions ($P=0.057$), pathogen defense ($P=0.029$), and regulation ($P=0.057$) in LCBM tissue (Supplementary Fig. 2c). Taken together, it is suspected that *EGFR* mutation may play a role in shaping the tumor microenvironment of brain metastatic

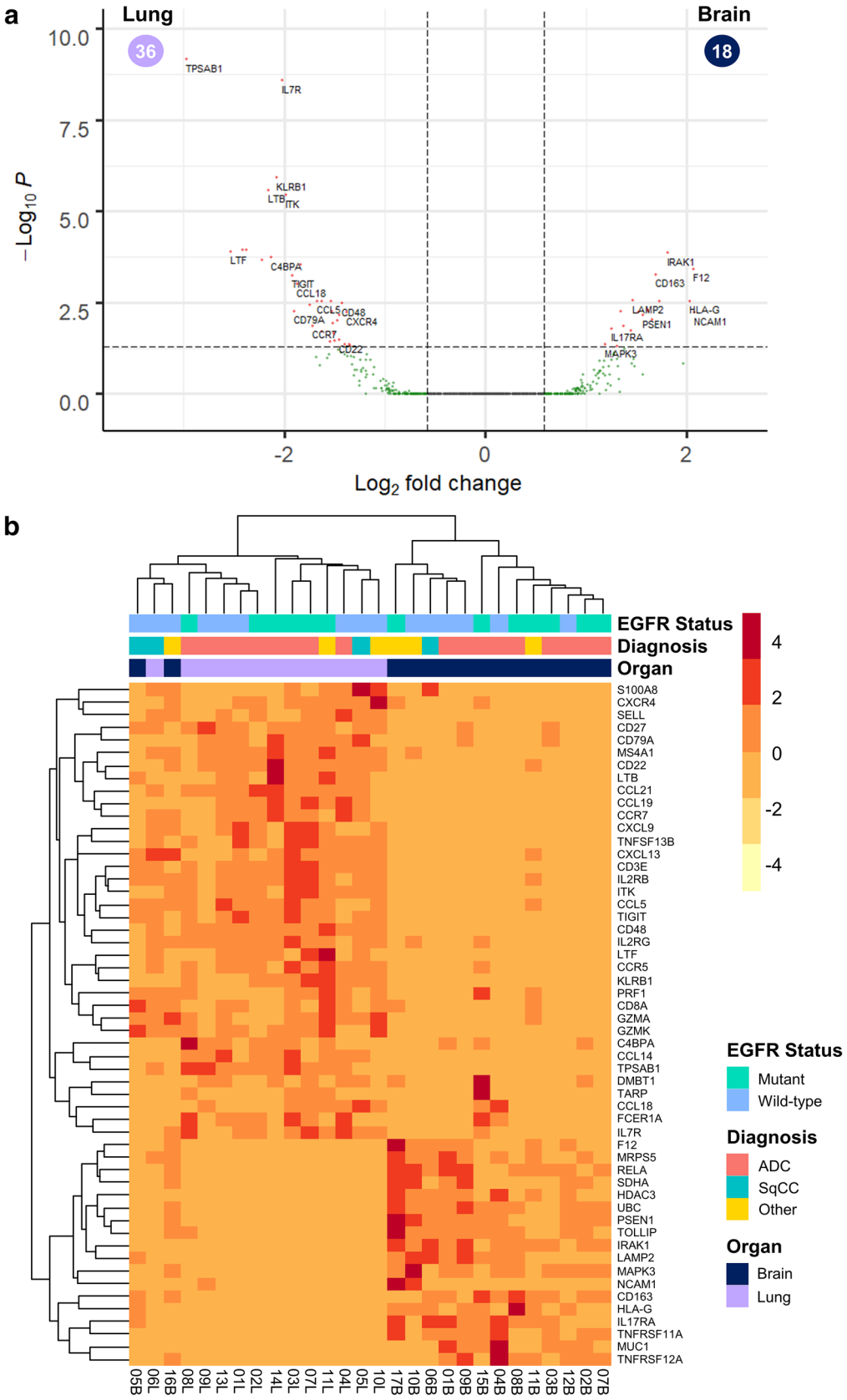
a
Lung
36
Brain
18
TPSAB1
IL7R
KLRB1
LTB
ITK
LTF
C4BPA
TIGIT
CCL18
CCL5
CD48
CD79A
CXCR4
CCR7
CD22
IRAK1
CD163
F12
LAMP2
HLA-G
PSEN1
NCAM1
IL17RA
MAPK3
$-\text{Log}_{10}\,P$
Log_2 fold change
b
EGFR Status
Diagnosis
Organ
S100A8
CXCR4
SELL
CD27
CD79A
MS4A1
CD22
LTB
CCL21
CCL19
CCR7
CXCL9
TNFSF13B
CXCL13
CD3E
IL2RB
ITK
CCL5
TIGIT
CD48
IL2RG
LTF
CCR5
KLRB1
PRF1
CD8A
GZMA
GZMK
C4BPA
CCL14
TPSAB1
DMBT1
TARP
CCL18
FCER1A
IL7R
F12
MRPS5
RELA
SDHA
HDAC3
UBC
PSEN1
TOLLIP
IRAK1
LAMP2
MAPK3
NCAM1
CD163
HLA-G
IL17RA
TNFRSF11A
MUC1
TNFRSF12A
05B 06L 16B 08L 09L 13L 01L 02L 14L 03L 07L 11L 04L 05L 10L 17B 10B 06B 01B 09B 15B 04B 08B 11B 03B 12B 02B 07B
EGFR Status
Mutant
Wild-type
Diagnosis
ADC
SqCC
Other
Organ
Brain
Lung

◂**Fig. 4** DEG exploration between primary lung cancer and LCBM reveals organ-dependent expression profile. **a** Volcano plot representing differentially expressed genes for primary lung tumor versus LCBM. Red and green dots, genes with or without statistical significance (fold change > 1.5 and adjusted $P < 0.05$). **b** Clustering heatmap of the 54 DEGs between the lung and brain

NSCLC, particularly adenocarcinoma, into a more immunologically active phenotype.

DEGs between primary lung cancer and LCBM

We explored the DEGs between primary lung cancer and LCBM. Eighteen genes were significantly upregulated in LCBM and 36 in primary lung cancer (Fig. 4a). In the cluster analysis based on these DEGs, brain metastases harboring mutated *EGFR* tended to cluster together (Fig. 4b). Among the DEGs, markers of T cells (*CD3E*) and B cells (*CD79A*) were upregulated in the primary lung tumor while those of M2 macrophage/microglia (*CD163*) and NK-cell/neural lineage (*NCAM1*) were upregulated in brain metastases. Furthermore, the anti-inflammatory markers *TOLLIP* and *HLA-G* [21, 22], were upregulated in LCBM. *S100A8*, which stimulates leukocyte infiltration and cytokine production during lung injury [23], was upregulated in the primary lung cancer. Although not statistically significant, the expression of most immune checkpoint molecules tended to be lower in brain metastatic lesions than in primary lung tumors, regardless of the alleged immune stimulatory- or inhibitory-role for each molecule (Supplementary Table 1).

We further searched for DEGs according to the *EGFR* mutation status. Among the lung samples, *EGFR*-mutated tumors showed upregulation of *LTK* and downregulation of *ADA*, *MAGEA3*, *MAGEB2*, *PBK*, and *USP9Y* (cutoff, fold change > 1.25). Among the brain tumors, *DMBT1* (fold change = 4.073, adjusted $P = 6.57E-05$) and *TGFB2* (fold change = 3.543, adjusted $P = 0.023$) were upregulated in those with *EGFR* mutation (cutoff, fold change > 1.25). Within each organ, no significant difference of immune checkpoint inhibitors was observed according to the *EGFR* mutation status.

Immune cell profiles: higher NK-cell density and enhanced M2 polarization of macrophages in LCBM

Next, we assessed the immune cell composition using the CIBERSORT and the NanoString method proposed by Danaher et al. [15, 16], and validated the results by immunohistochemistry in the extended cohort. NCR1, iNOS and CD163 were used as markers of NK-cells, M1- and M2-macrophages, respectively [24, 25]. The proportions of most immune cell subsets were reduced in LCBM compared to primary lung cancer. However, the proportion of M2-macrophages was higher in the brain (Fig. 5a, upper; Fig. 5b). The relative proportions of macrophages and CD56dim-NK-cells among the total TILs were significantly higher in LCBM (Fig. 5a, lower). The ratio of M1- to M2-macrophages and that of NK-cells to total T cells were also significantly higher in LCBM (Fig. 5a, lower; Fig. 5c, d, e; Supplementary Fig. 3). Within each organ, there was no significant difference in the proportions of immune cell types between *EGFR*–mutated and wild-type cases (Supplementary Fig. 4a–d). These findings demonstrate that LCBM tumors generally have reduced immune cell infiltration but increased proportions of NK-cells and M2-polarized tumor-associated macrophages (TAMs).

Discussion

Previous studies comparing primary lung cancer and LCBM showed good agreement in terms of mutations of major oncogenic drivers but different copy number alterations of key genes including *MYC* and *CDKN2A/B* [26, 27]. Infiltration by T cells was reduced and that by macrophages was increased in LCBM, determined by gene expression analysis [26]. In this study, we investigated the immunologic landscape of primary lung cancer and LCBM to assess the effect of tumor-involved organs and *EGFR* mutation status on the tumor immune-microenvironment and to discover potential immunotherapeutic targets.

EGFR mutation in NSCLC is associated with a lower tumor mutation burden, PD-L1 expression, and T cell infiltration [19, 28]. In this study, clustering analysis with the NanoString panel profiling revealed that the primary lung cancer and LCBM samples formed distinct clusters, and *EGFR* wild-type and mutated cases tended to be distinct within each organ cluster, particularly in the brain. Immune pathway scoring showed that the immune reaction potential was consistently lower in LCBM tissue compared to primary lung tumor, irrespective of *EGFR* mutation status. Interestingly, while *EGFR* mutation status did not affect the immune pathway scores of primary lung tumors, the overall immune pathway scores of the LCBM cases were higher in the *EGFR*-mutated cases, indicating an immunogenic phenotype. Therefore, the effect of *EGFR* mutation on the tumor immune-microenvironment may vary among organs and the *EGFR* mutation of a tumor might shape the tumor immune-microenvironment of metastases.

Recently, it has been suggested that there may be differences in tumor immune-microenvironment depending on the type of *EGFR* mutations. Between the two most

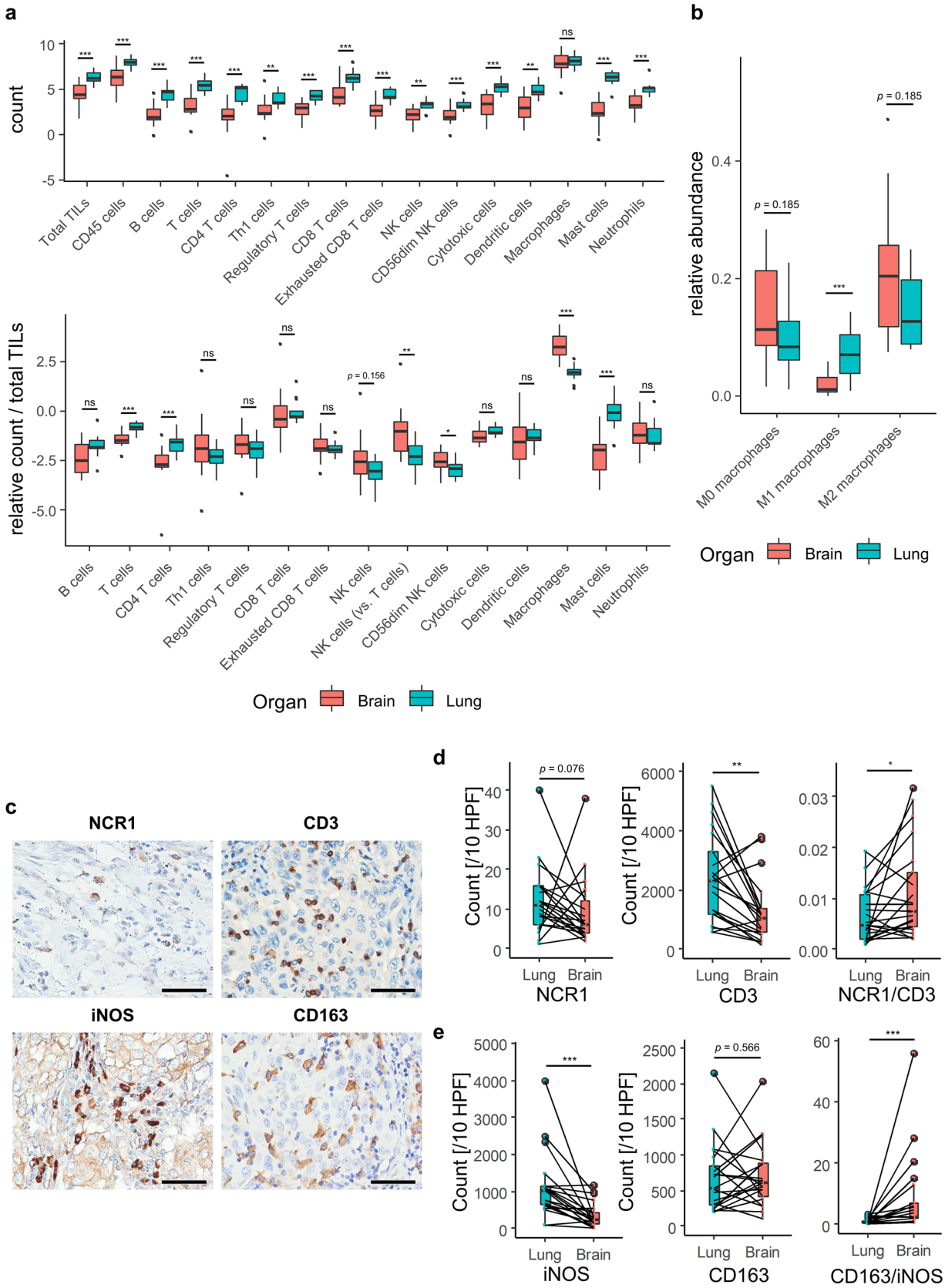
a
count
Total TILs
CD45 cells
B cells
T cells
CD4 T cells
Th1 cells
Regulatory T cells
CD8 T cells
Exhausted CD8 T cells
NK cells
CD56dim NK cells
Cytotoxic cells
Dendritic cells
Macrophages
Mast cells
Neutrophils
relative count / total TILs
NK cells (vs. T cells)
Organ
Brain
Lung
b
relative abundance
p = 0.185
M0 macrophages
M1 macrophages
M2 macrophages
c
NCR1
CD3
iNOS
CD163
d
Count [/10 HPF]
p = 0.076
NCR1
CD3
NCR1/CD3
e
p = 0.566
iNOS
CD163
CD163/iNOS

◂**Fig. 5** Higher NK-cell density and enhanced M2 polarization of macrophages in LCBM. **a** Immune cell profiling with the NanoString method. Cell count score for individual cell type (upper) and relative abundance per total tumor infiltrating leukocytes (TILs; lower) are plotted (Mann–Whitney U test). Relative proportion of NK-cells per TILs or T cells are also shown. Total TILs are defined as the mean value of the count score for B cells, T cells, CD45-positive cells, macrophages, and cytotoxic cells. **b** Cell profile of macrophages analyzed with CIBERSORT algorithm (Mann–Whitney *U* test). **c** Representative immunohistochemical images of NCR1, CD3, iNOS, and CD163. Scale bar, 50 µm. **d** Numbers of NCR1-positive cells, CD3-positive cells and their ratio (Wilcoxon signed–rank test). **e** Cell counts for iNOS-positive cells, CD163-positive cells and their ratio (Wilcoxon signed–rank test). *, $P<0.05$; **, $P<0.01$; ***, $P<0.001$; *ns* not significant

common sensitizing mutation cases, i.e., *EGFR* exon 19 deletion and exon 21 L858R point mutation cases, there were differences in tumor mutational burden, and the responses to ICI, which were worse in patients with exon 19 deletion [28, 29]. Therefore, we also analyzed DEGs between L858R point mutation and exon 19 deletion patients in lung and brain, respectively. Within lung samples, no statistically significant DEG was discovered. Within LCBM cases, one gene (*IL8*) was upregulated in exon 19 deleted patients (fold change = 5.86, adjusted $P = 0.018$). Further studies are warranted to unveil the underlying immunologic differences among these specific oncogenic mutational profiles.

The expression levels of some genes differed between *EGFR*-wild-type and -mutant cases. The expression of *LTK*, a close homolog of *ALK* associated with tumorigenesis of acute myeloid leukemia [30], was higher in *EGFR*-mutated lung tumors. *TGFB2*, which is associated with tumor progression by promoting cancer cell invasion and epithelial-mesenchymal transition [31], was upregulated in *EGFR*-mutated LCBM samples. Improved patient survival was observed in a phase III trial of a TGF-β2 antisense-modified NSCLC tumor cell vaccine, and other drugs targeting the TGF-β pathway are under clinical investigation [32, 33]. The utility of targeting these molecules in *EGFR*-mutated lung cancer remains to be evaluated.

Based on immune cell deconvolution analysis and immunohistochemical validation, the macrophage population in LCBM was polarized to the M2 phenotype compared to primary lung cancer. TAMs typically exhibit an M2-like phenotype and exert pro-tumoral and anti-inflammatory effects [34]. TAM is the key element of the microenvironment in glioma and blocking of TAMs with an anti-*CSF-1R* antibody induced glioma regression [35, 36]. *CSF1*, a ligand for *CSF-1R*, is also expressed in lung cancer and is associated with distant organ metastasis [37]. Thus, the therapeutic effect of *CSF-1R* blockade or other approaches targeting M2-TAM in LCBM should be explored.

We also found that the counts of most immune cell types were smaller in the brain, reflecting the alleged poor immune repertoire of the CNS [38]. However, regarding the relative proportion in total TIL counts, the density of mast cells and T cells were higher in the primary lung lesion, whereas LCBM samples were highly infiltrated by macrophages and CD56dim-NK-cells. The total NK-cell to T cell ratio was also higher in LCBM compared to the primary lung tumor. These findings implicate that the innate immune system may be closely related to the anti-tumor immune response to LCBM. CD56dim-NK-cells are major NK-cell subset responsible for effective cytolytic activity and secretion of proinflammatory cytokines [39–41]. Thus, immunotherapeutic strategies targeting these cells may be effective for LCBM. Of note, DEG analysis showed that the expression of *HLA-G* was upregulated in LCBM. HLA-G is a non-classical HLA class I molecule that suppresses various immune cells in the tumor microenvironment [21]. In an in vitro study using NSCLC cells, *HLA-G* inhibited the cytotoxic function of NK-cells [42]. The growth potential of *HLA-G*-positive tumor was reversed by a monoclonal antibody in a murine in vivo model [43]. Therefore, our findings suggest that HLA-G contributes to the immunosuppressive phenotype of LCBM and may serve as a potential therapeutic target which may enhance the cytotoxic effect of NK-cells by inhibiting *HLA-G* in tumor cells.

Responsiveness to ICI differs between extracranial and intracranial tumors [5]. Reduced infiltration of PD-1-positive TILs in LCBM was suggested as an explanation for the resistance to ICI [9]. In this study, there was no difference in *PDCD1* (*PD-1*) or *CD274* (*PD-L1*) expression between brain and lung tumor tissues; however, the IFN-γ signature score, a predictor of the clinical response to ICI [13], was lower in LCBM. These findings indicate that differences in anti-tumor immunity that are obscure at the single-gene-expression level can be revealed by using a signature score consisting of multiple genes [13].

However, our study is limited by the small number of cases analyzed in the NanoString panel analysis. Because the study used FFPE tissue and a number of the samples had been stored for more than 5 years, a large number of cases were excluded due to the inadequate quality of the extracted RNA. In addition, we were unable to reveal oncogenic alteration in 9 out of 17 patients in the NanoString cohort, limiting the evaluation of the immune microenvironment in patients with oncogenic alterations encompassing genes other than *EGFR, KRAS*, or *ALK*. Nevertheless, to the best of our knowledge, this is the first study of the immune landscape of matched primary and brain lung cancer metastases in terms of *EGFR* mutation status. We also validated the increased proportion of NK-cells and M2-macrophages in the brain by immunohistochemistry and explored potential

treatment strategies targeting NK-cells via their interaction with the *HLA-G* pathway in LCBM.

Conclusion

We found organ-specific and *EGFR*-dependent differences in the tumor immune-microenvironment between primary NSCLC and its brain metastases. Brain metastases showed an immunosuppressive phenotype in terms of immune-related pathways and the composition of immune cell infiltrates. However, LCBM had a unique immune cellular component and gene expression, which may have immunotherapeutic implications. The differences in the immune reaction of LCBM according to *EGFR* mutation status should be considered when treating patients with *EGFR*-mutated lung cancer with brain metastasis.

Acknowledgements The authors thank Dr. Yeon Duk Woo (Department of Biomedical Sciences, Seoul National University College of Medicine, Seoul, Republic of Korea) for manuscript editing.

Author contributions DHC, YKJ and YAK designed and supervised the study. SGS, SK, JK, JY and BH performed experiments and acquired the data. SGS, SK, YAK and YKJ analyzed the results. SGS and YKJ made the figures and tables. SGS, YKJ and DHC wrote the manuscript. All authors read and approved the final manuscript.

Funding This work was supported by the Basic Research Program through the National Research Foundation of Korea (NRF) funded by the Ministry of Science and ICT (MSIT) (grant No.: 2020R1A4A1017515) and the Basic Science Research through the NRF funded by the Ministry of Education, Science and Technology (MEST) Program (grant No.: NRF-2016R1D1A1B01015964), Republic of Korea.

Data availability The gene-expression data were uploaded on the Gene Expression Omnibus (GEO) database (https://www.ncbi.nlm.nih.gov/geo/query/acc.cgi?acc=GSE161116).

Compliance with ethical standards

Conflict of interest The authors declare no conflict of interest.

Ethical approval This study was approved by the Institutional Review Board of SNUH (No. 1404–102-572) and was performed in accordance with the World Medical Association Declaration of Helsinki. The requirement for informed consent was waived because of the retrospective nature of the study.

References

1. Cagney DN, Martin AM, Catalano PJ, Redig AJ, Lin NU, Lee EQ, Wen PY, Dunn IF, Bi WL, Weiss SE, Haas-Kogan DA, Alexander BM, Aizer AA (2017) Incidence and prognosis of patients with brain metastases at diagnosis of systemic malignancy: a population-based study. Neuro Oncol 19(11):1511–1521. https://doi.org/10.1093/neuonc/nox077
2. Riihimaki M, Hemminki A, Fallah M, Thomsen H, Sundquist K, Sundquist J, Hemminki K (2014) Metastatic sites and survival in lung cancer. Lung Cancer 86(1):78–84. https://doi.org/10.1016/j.lungcan.2014.07.020
3. Deeken JF, Loscher W (2007) The blood-brain barrier and cancer: transporters, treatment, and Trojan horses. Clin Cancer Res 13(6):1663–1674. https://doi.org/10.1158/1078-0432.CCR-06-2854
4. Abdallah SM, Wong A (2018) Brain metastases in non-small-cell lung cancer: are tyrosine kinase inhibitors and checkpoint inhibitors now viable options? Curr Oncol 25(Suppl 1):S103–S114. https://doi.org/10.3747/co.25.3733
5. Goldberg SB, Schalper KA, Gettinger SN, Mahajan A, Herbst RS, Chiang AC, Lilenbaum R, Wilson FH, Omay SB, Yu JB, Jilaveanu L, Tran T, Pavlik K, Rowen E, Gerrish H, Komlo A, Gupta R, Wyatt H, Ribeiro M, Kluger Y, Zhou G, Wei W, Chiang VL, Kluger HM (2020) Pembrolizumab for management of patients with NSCLC and brain metastases: long-term results and biomarker analysis from a non-randomised, open-label, phase 2 trial. Lancet Oncol 21(5):655–663. https://doi.org/10.1016/S1470-2045(20)30111-X
6. Cacho-Diaz B, Garcia-Botello DR, Wegman-Ostrosky T, Reyes-Soto G, Ortiz-Sanchez E, Herrera-Montalvo LA (2020) Tumor microenvironment differences between primary tumor and brain metastases. J Transl Med 18(1):1. https://doi.org/10.1186/s12967-019-02189-8
7. Komohara Y, Ohnishi K, Kuratsu J, Takeya M (2008) Possible involvement of the M2 anti-inflammatory macrophage phenotype in growth of human gliomas. J Pathol 216(1):15–24. https://doi.org/10.1002/path.2370
8. Sampson JH, Gunn MD, Fecci PE, Ashley DM (2020) Brain immunology and immunotherapy in brain tumours. Nat Rev Cancer 20(1):12–25. https://doi.org/10.1038/s41568-019-0224-7
9. Kim R, Keam B, Kim S, Kim M, Kim SH, Kim JW, Kim YJ, Kim TM, Jeon YK, Kim DW, Chung DH, Lee JS, Heo DS (2019) Differences in tumor microenvironments between primary lung tumors and brain metastases in lung cancer patients: therapeutic implications for immune checkpoint inhibitors. BMC Cancer 19(1):19. https://doi.org/10.1186/s12885-018-5214-8
10. Mansfield AS, Aubry MC, Moser JC, Harrington SM, Dronca RS, Park SS, Dong H (2016) Temporal and spatial discordance of programmed cell death-ligand 1 expression and lymphocyte tumor infiltration between paired primary lesions and brain metastases in lung cancer. Ann Oncol 27(10):1953–1958. https://doi.org/10.1093/annonc/mdw289
11. Cesano A (2015) nCounter((R)) pancancer immune profiling panel (NanoString Technologies Inc, Seattle, WA). J Immunother Cancer 3:42. https://doi.org/10.1186/s40425-015-0088-7
12. Love MI, Huber W, Anders S (2014) Moderated estimation of fold change and dispersion for RNA-seq data with DESeq2. Genome Biol 15(12):550. https://doi.org/10.1186/s13059-014-0550-8
13. Ayers M, Lunceford J, Nebozhyn M, Murphy E, Loboda A, Kaufman DR, Albright A, Cheng JD, Kang SP, Shankaran V, Piha-Paul SA, Yearley J, Seiwert TY, Ribas A, McClanahan TK (2017) IFN-gamma-related mRNA profile predicts clinical response to PD-1 blockade. J Clin Invest 127(8):2930–2940. https://doi.org/10.1172/JCI91190
14. Tomfohr J, Lu J, Kepler TB (2005) Pathway level analysis of gene expression using singular value decomposition. BMC Bioinform 6:225. https://doi.org/10.1186/1471-2105-6-225
15. Danaher P, Warren S, Dennis L, D'Amico L, White A, Disis ML, Geller MA, Odunsi K, Beechem J, Fling SP (2017) Gene

expression markers of tumor infiltrating leukocytes. J Immunother Cancer 5:18. https://doi.org/10.1186/s40425-017-0215-8
16. Newman AM, Liu CL, Green MR, Gentles AJ, Feng W, Xu Y, Hoang CD, Diehn M, Alizadeh AA (2015) Robust enumeration of cell subsets from tissue expression profiles. Nat Methods 12(5):453–457. https://doi.org/10.1038/nmeth.3337
17. Bindea G, Mlecnik B, Tosolini M, Kirilovsky A, Waldner M, Obenauf AC, Angell H, Fredriksen T, Lafontaine L, Berger A, Bruneval P, Fridman WH, Becker C, Pages F, Speicher MR, Trajanoski Z, Galon J (2013) Spatiotemporal dynamics of intratumoral immune cells reveal the immune landscape in human cancer. Immunity 39(4):782–795. https://doi.org/10.1016/j.immuni.2013.10.003
18. Lee JK, Lee J, Kim S, Kim S, Youk J, Park S, An Y, Keam B, Kim DW, Heo DS, Kim YT, Kim JS, Kim SH, Lee JS, Lee SH, Park K, Ku JL, Jeon YK, Chung DH, Park PJ, Kim J, Kim TM, Ju YS (2017) Clonal history and genetic predictors of transformation into small-cell carcinomas from lung adenocarcinomas. J Clin Oncol 35(26):3065–3074. https://doi.org/10.1200/JCO.2016.71.9096
19. Dong ZY, Zhang JT, Liu SY, Su J, Zhang C, Xie Z, Zhou Q, Tu HY, Xu CR, Yan LX, Li YF, Zhong WZ, Wu YL (2017) EGFR mutation correlates with uninflamed phenotype and weak immunogenicity, causing impaired response to PD-1 blockade in non-small cell lung cancer. Oncoimmunology 6(11):e1356145. https://doi.org/10.1080/2162402X.2017.1356145
20. Isomoto K, Haratani K, Hayashi H, Shimizu S, Tomida S, Niwa T, Yokoyama T, Fukuda Y, Chiba Y, Kato R, Tanizaki J, Tanaka K, Takeda M, Ogura T, Ishida T, Ito A, Nakagawa K (2020) Impact of EGFR-TKI Treatment on the tumor immune microenvironment in EGFR mutation-positive non-small cell lung cancer. Clin Cancer Res 26(8):2037–2046. https://doi.org/10.1158/1078-0432.CCR-19-2027
21. Lin A, Yan WH (2018) Heterogeneity of HLA-G expression in cancers: facing the challenges. Front Immunol 9:2164. https://doi.org/10.3389/fimmu.2018.02164
22. Humbert-Claude M, Duc D, Dwir D, Thieren L, Sandstrom von Tobel J, Begka C, Legueux F, Velin D, Maillard MH, Do KQ, Monnet-Tschudi F, Tenenbaum L (2016) Tollip, an early regulator of the acute inflammatory response in the substantia nigra. J Neuroinflammation 13(1):303. https://doi.org/10.1186/s12974-016-0766-5
23. Wang S, Song R, Wang Z, Jing Z, Wang S, Ma J (2018) S100A8/A9 in inflammation. Front Immunol 9:1298. https://doi.org/10.3389/fimmu.2018.01298
24. Hu VH, Luthert PJ, Derrick T, Pullin J, Weiss HA, Massae P, Mtuy T, Makupa W, Essex D, Mabey DC, Bailey RL, Holland MJ, Burton MJ (2016) Immunohistochemical analysis of scarring trachoma indicates infiltration by natural killer and undefined CD45 negative cells. PLoS Negl Trop Dis 10(5):e0004734. https://doi.org/10.1371/journal.pntd.0004734
25. Lisi L, Ciotti GM, Braun D, Kalinin S, Curro D, Dello Russo C, Coli A, Mangiola A, Anile C, Feinstein DL, Navarra P (2017) Expression of iNOS, CD163 and ARG-1 taken as M1 and M2 markers of microglial polarization in human glioblastoma and the surrounding normal parenchyma. Neurosci Lett 645:106–112. https://doi.org/10.1016/j.neulet.2017.02.076
26. Kudo Y, Haymaker C, Zhang J, Reuben A, Duose DY, Fujimoto J, Roy-Chowdhuri S, Solis Soto LM, Dejima H, Parra ER, Mino B, Abraham R, Ikeda N, Vaporcyan A, Gibbons D, Zhang J, Lang FF, Luthra R, Lee JJ, Moran C, Huse JT, Kadara H, Wistuba II (2019) Suppressed immune microenvironment and repertoire in brain metastases from patients with resected non-small-cell lung cancer. Ann Oncol 30(9):1521–1530. https://doi.org/10.1093/annonc/mdz207
27. Shih DJH, Nayyar N, Bihun I, Dagogo-Jack I, Gill CM, Aquilanti E, Bertalan M, Kaplan A, D'Andrea MR, Chukwueke U, Ippen FM, Alvarez-Breckenridge C, Camarda ND, Lastrapes M, McCabe D, Kuter B, Kaufman B, Strickland MR, Martinez-Gutierrez JC, Nagabhushan D, De Sauvage M, White MD, Castro BA, Hoang K, Kaneb A, Batchelor ED, Paek SH, Park SH, Martinez-Lage M, Berghoff AS, Merrill P, Gerstner ER, Batchelor TT, Frosch MP, Frazier RP, Borger DR, Iafrate AJ, Johnson BE, Santagata S, Preusser M, Cahill DP, Carter SL, Brastianos PK (2020) Genomic characterization of human brain metastases identifies drivers of metastatic lung adenocarcinoma. Nat Genet 52(4):371–377. https://doi.org/10.1038/s41588-020-0592-7
28. Offin M, Rizvi H, Tenet M, Ni A, Sanchez-Vega F, Li BT, Drilon A, Kris MG, Rudin CM, Schultz N, Arcila ME, Ladanyi M, Riely GJ, Yu H, Hellmann MD (2019) Tumor mutation burden and efficacy of EGFR-tyrosine kinase inhibitors in patients with EGFR-mutant lung cancers. Clin Cancer Res 25(3):1063–1069. https://doi.org/10.1158/1078-0432.CCR-18-1102
29. Hastings K, Yu HA, Wei W, Sanchez-Vega F, DeVeaux M, Choi J, Rizvi H, Lisberg A, Truini A, Lydon CA, Liu Z, Henick BS, Wurtz A, Cai G, Plodkowski AJ, Long NM, Halpenny DF, Killam J, Oliva I, Schultz N, Riely GJ, Arcila ME, Ladanyi M, Zelterman D, Herbst RS, Goldberg SB, Awad MM, Garon EB, Gettinger S, Hellmann MD, Politi K (2019) EGFR mutation subtypes and response to immune checkpoint blockade treatment in non-small-cell lung cancer. Ann Oncol 30(8):1311–1320. https://doi.org/10.1093/annonc/mdz141
30. Muller-Tidow C, Schwable J, Steffen B, Tidow N, Brandt B, Becker K, Schulze-Bahr E, Halfter H, Vogt U, Metzger R, Schneider PM, Buchner T, Brandts C, Berdel WE, Serve H (2004) High-throughput analysis of genome-wide receptor tyrosine kinase expression in human cancers identifies potential novel drug targets. Clin Cancer Res 10(4):1241–1249. https://doi.org/10.1158/1078-0432.ccr-0954-03
31. Pickup M, Novitskiy S, Moses HL (2013) The roles of TGFbeta in the tumour microenvironment. Nat Rev Cancer 13(11):788–799. https://doi.org/10.1038/nrc3603
32. Giaccone G, Bazhenova LA, Nemunaitis J, Tan M, Juhasz E, Ramlau R, van den Heuvel MM, Lal R, Kloecker GH, Eaton KD, Chu Q, Dunlop DJ, Jain M, Garon EB, Davis CS, Carrier E, Moses SC, Shawler DL, Fakhrai H (2015) A phase III study of belagenpumatucel-L, an allogeneic tumour cell vaccine, as maintenance therapy for non-small cell lung cancer. Eur J Cancer 51(16):2321–2329. https://doi.org/10.1016/j.ejca.2015.07.035
33. Akhurst RJ, Hata A (2012) Targeting the TGFbeta signalling pathway in disease. Nat Rev Drug Discov 11(10):790–811. https://doi.org/10.1038/nrd3810
34. Guadagno E, Presta I, Maisano D, Donato A, Pirrone CK, Cardillo G, Corrado SD, Mignogna C, Mancuso T, Donato G, De Basso DCM, Malara M (2018) Role of macrophages in brain tumor growth and progression. Int J Mol Sci. https://doi.org/10.3390/ijms19041005
35. Charles NA, Holland EC, Gilbertson R, Glass R, Kettenmann H (2012) The brain tumor microenvironment. Glia 60(3):502–514. https://doi.org/10.1002/glia.21264
36. Pyonteck SM, Akkari L, Schuhmacher AJ, Bowman RL, Sevenich L, Quail DF, Olson OC, Quick ML, Huse JT, Teijeiro V, Setty M, Leslie CS, Oei Y, Pedraza A, Zhang J, Brennan CW, Sutton JC, Holland EC, Daniel D, Joyce JA (2013) CSF-1R inhibition alters macrophage polarization and blocks glioma progression. Nat Med 19(10):1264–1272. https://doi.org/10.1038/nm.3337
37. Hung JY, Horn D, Woodruff K, Prihoda T, LeSaux C, Peters J, Tio F, Abboud-Werner SL (2014) Colony-stimulating factor 1 potentiates lung cancer bone metastasis. Lab Invest 94(4):371–381. https://doi.org/10.1038/labinvest.2014.1
38. Morimoto K, Nakajima K (2019) Role of the immune system in the development of the central nervous system. Front Neurosci 13:916. https://doi.org/10.3389/fnins.2019.00916

39. Moretta L (2010) Dissecting CD56dim human NK cells. Blood 116(19):3689–3691. https://doi.org/10.1182/blood-2010-09-303057
40. Geller MA, Miller JS (2011) Use of allogeneic NK cells for cancer immunotherapy. Immunotherapy 3(12):1445–1459. https://doi.org/10.2217/imt.11.131
41. Golan I, de Rodriguez FL, Costoya JA (2018) NK cell-based glioblastoma immunotherapy. Cancers (Basel). https://doi.org/10.3390/cancers10120522
42. Lin A, Zhu CC, Chen HX, Chen BF, Zhang X, Zhang JG, Wang Q, Zhou WJ, Hu W, Yang HH, Xu HH, Yan WH (2010) Clinical relevance and functional implications for human leucocyte antigen-g expression in non-small-cell lung cancer. J Cell Mol Med 14(9):2318–2329. https://doi.org/10.1111/j.1582-4934.2009.00858.x
43. Agaugue S, Carosella ED, Rouas-Freiss N (2011) Role of HLA-G in tumor escape through expansion of myeloid-derived suppressor cells and cytokinic balance in favor of Th2 versus Th1/Th17. Blood 117(26):7021–7031. https://doi.org/10.1182/blood-2010-07-294389

Affiliations

Seung Geun Song[1] · Sehui Kim[1,2] · Jaemoon Koh[1,2] · Jeemin Yim[1] · Bogyeong Han[1] · Young A. Kim[3] · Yoon Kyung Jeon[1,4] · Doo Hyun Chung[1,2]

1 Department of Pathology, Seoul National University College of Medicine, 101 Daehak-ro, Jongno-gu, Seoul 03080, Republic of Korea

2 Laboratory of Immune Regulation, Department of Biomedical Sciences, Seoul National University College of Medicine, 101 Daehak-ro, Jongno-gu, Seoul 03080, Republic of Korea

3 Department of Pathology, Seoul Metropolitan Government-Seoul National University Boramae Medical Center, Seoul, Republic of Korea

4 Cancer Research Institute, Seoul National University, Seoul, Republic of Korea